EARTH'S CRYOSPHERE
SCIENTIFIC JOURNAL

Earth's Cryosphere, 2022, vol. XXVI, No. 1, pp. 19–31 http://earthcryosphere.ru/

CRYOLITHOGENESIS

TRACES OF CRYOGENIC PROCESSES IN THE LATE PLEISTOCENE SEDIMENTS OF THE PUR-TAZ INTERFLUVE (WEST SIBERIA)

E.A. Slagoda[1–3], A.A. Novoselov[2], E.S. Koroleva[1], A.O. Kuznetsova[1], V.I. Butakov[3], Ya.V. Tikhonravova[4], E.P. Zazovskaya[5]

[1] *Earth Cryosphere Institute, Tyumen Scientific Center, Siberian Branch of the Russian Academy of Sciences, Malygina str. 86, Tyumen, 625026 Russia; eslagoda@ikz.ru*
[2] *University of Tyumen, Volodarskogo str. 6, Tyumen, 625003 Russia*
[3] *Tyumen Industrial University, Volodarskogo str. 38, Tyumen, 625000 Russia*
[4] *Melnikov Permafrost Institute, Siberian Branch of the Russian Academy of Sciences, Merzlotnaya str. 36, Yakutsk, 677010 Russia*
[5] *Institute of Geography, Russian Academy of Sciences, Staromonetnyi per. 29, Moscow, 119017 Russia*

Reconstruction of paleoenvironmental conditions, genesis of sediments, and permafrost evolution, as well as identification of cryogenic and paleocryogenic formations from sediment cores are among key scientific problems of cryolithology. We have analyzed grain-size distribution, geochemistry, and water content of sediments from the permafrost section in the north of the Pur-Taz interfluve (West Siberia). Moreover, we have described the floristic composition of plant remains, their age and the cryostructures found within these sediments. Optical and electron microscopy have been applied to reveal the micromorphological features of thin sections and rock specimens. Based on the sediment core data from the borehole, we have established the alluvial, lacustrine, and colluvial geneses of sediments. Furthermore, we have reconstructed the conditions of sediment deposition in this area and have established the Karginsky age of these sediments. This age corresponds to the third lacustrine–alluvial plain in the lower course of the Taz River. The conditions of the early diagenetic transformation of sediments, as well as epicryogenic and syncryogenic structure types have been reconstructed based on cryogenic and post-cryogenic formations, cryostructures, microstructure, and authigenic minerals. We have also reconstructed the Late Pleistocene sequences of freeze–thaw cycles in the upper part of the permafrost section of the Pur-Taz interfluve.

Keywords: *cryogenic structure, post-cryogenic formations, genesis, age, composition, microstructure, authigenic minerals of sediments*

INTRODUCTION

The determination of the initial freezing type (syngenetic or epigenetic) of thawed or refrozen sediments, as well as traces of consequent freeze–thaw cycles in the upper permafrost section are among the major problems of cryolithology. Traces of sedimentary, early diagenetic, and cryogenic processes are often present within the same geological unit. Therefore, it is required to consider different features for determining the dynamics of deposition and its environment, freezing type and thawing traces while interpreting the lithology and elements of cryogenic and post-cryogenic structure. These features can help in the reconstruction of synchronous and superimposed transformations. The interpretation of the section using the borehole data only in case of exposure absence is probabilistic, because it is impossible to obtain a full morphological pattern and details of cryogenic and post-cryogenic formation structures.

We carried out cryolithological research aimed at studying the consequences of staged changes of frozen/thawed states in the upper permafrost section of the Pur-Taz interfluve in West Siberia. Our sediment core data allowed us to determine (1) the genesis, deposition environment, and age of sediments; (2) stages and types of freezing/thawing in the section with sufficient confidence; and (3) their interrelationships with paleoenvironmental changes in the Late Pleistocene.

The area of our study belongs to the Kharasavey-Novy Urengoy subzone of the continental geocryological province of the West Siberian Plate and is characterized by continuous syncryogenic and epicryogenic permafrost [*Ershov, 1989*]. The area is located in the northeast of the Pur-Taz interfluve, 20 km from the Tazovsky settlement. It belongs to the southern tundra subzone within the plain with absolute heights ranging from 10–16 to 35–60 m a.s.l., poorly dissected topography, and polygonal microtopography on elevated ridges (Fig. 1). The plain is dissected by river valleys, lakes, and thermokarst de-

pressions (khasyreys) with polygonal peat plateaus [*Trofimov et al., 1987*]. Ice wedges in peatlands, thermokarst and thermoerosional depressions, bulgunnyakhs, polygonal microtopography, and frost boils are widespread in this area [*Vasil'chuk and Vasil'chuk, 2016; Tikhonravova et al., 2020*]. Initially ground veins, single and multi-tiered pseudomorphs and distinct polygonal topography resulting from the melting of ice wedges are evidences of permafrost evolution in this area. Pseudomorphs are located within the thawed and frozen epicryogenic Late Pleistocene sediments [*Shmelev, 1966; Zykina et al., 2017*]. Little is known about post-cryogenic formations and micromorphology of sediments related to cryogenic processes in the section of the Pur-Taz interfluve.

OBJECT AND METHODS

The study object is sediment core sampled from borehole 1-16 drilled on an elevated polygonal surface (28 m a.s.l.) within the basin of left tributaries of the Taz River in its lower course. The 8.8-m-deep borehole penetrated the Late Pleistocene sands and loamy sands in the frozen (with the temperature of –3 °C) [*Khomutov et al., 2019*]) and seasonally thawed (0–1.4 m) states. Pits 1/17 and 1/18 on the slope with polygons and numerous mineral frost boils (Fig. 1*B*) exposed thawed sediments to a depth of 2.4 m [*Slagoda et al., 2019*]. The description of the geological section is given in Table 1 and Fig. 2.

We studied the cryogenic structure of the core and determined the water content, grain-size distribution, ionic composition of the water extract from the sediments, and the content of plant remains in the core samples of 59–94 mm in diameter. Sedimentary, cryogenic, and post-cryogenic structure elements were identified within the undisturbed frozen and thawed parts of the core.

Grain-size distribution in 21 samples was measured using a Mastersizer 3000 laser diffraction particle-size analyzer [*Kurchatova and Rogov, 2014*]. We determined the (i) mineralogical composition, (ii) sedimentary and superimposed post-cryogenic microstructures, (iii) shape of terrigenous particles, and (iv) authigenic minerals using an Olympus-BX53M-TRF polarizing microscope (for seven thin sections) and a Hitachi TM3000 scanning electron microscope (SEM) combined with SwiftED3000 energy dispersive X-ray spectrometer [*Kurchatova and Rogov, 2020*].

Plant remains extracted from the sediment core were identified using microscopy and reference col-

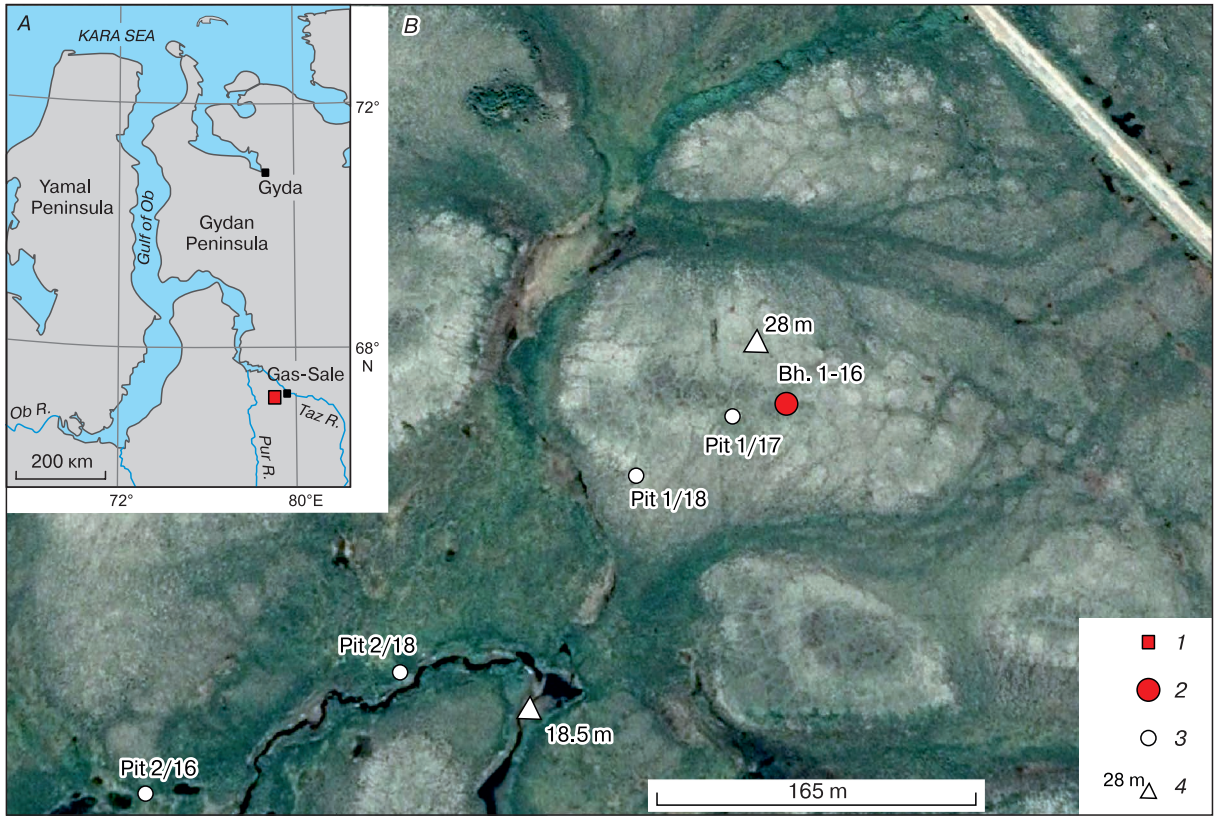

Fig. 1. Study area in the northeast of the Pur-Taz interfluve.

A – overview map; *B* – scheme of pit locations (Google Earth, Landsat [*2020*] as background): (*1*) study site, (*2*) borehole, (*3*) pits, and (*4*) elevation marks.

Table 1. **Summary description of sediments on the Pur-Taz interfluve in samples from borehole 1-16 and soil pits 1/17 and 1/18**

Layer number; depth, m	Sediment description
7, 0.4–0.0	Frequent interbedding of loamy sand and silty sand with crumpled bedding, lenticular-reticulate post-cryogenic structure, cryoturbation, and modern roots. Loamy sand and sand compose intrusions and mud boils on the surface. Two tiers of mud boils displaced downslope and inclined humus veins were exposed in this layer in pits 1/17 and 1/18. The soil between bare surface of mud boils represents a humified reddish brown loamy sand (to a depth of 0.2 m) roots of modern dwarf shrubs, mosses and lichen residues, and humus tongues of up to 0.5 m in length. The entire layer is thawed. Water content W = 16–18 %
6, 2–0.4	Gray loamy sand with interlayers of yellowish and light gray silty sands, with numerous dark brown mottles along decomposed plant roots. The bedding is wavy, tilted in the lower part parallel to the uneven sloping surface of the underlying layer and indistinctly subhorizontal in the upper part. Vertical streaks and mottles of ocherous and yellow-colored masses enriched in iron compounds. Layers of 1–10 cm in thickness have numerous folds, displacements, interpenetrations, discontinuities, and wavy boundaries. The top of the layer is uneven, complicated by the upward intrusion of loamy sand and by the ends of humus tongues from the top. In the borehole, sediments are in the frozen state from a depth of 0.4 m and have massive cryogenic structure; in the upper part of the layer, thin lenticular structure parallel to the surface, W = 36–40 %. On the slope, the layer is in a thawed state (to a depth of 2.4 m, pit 1/17)
5, 4.25–2.0	Light gray, brownish and yellowish fine sand and silty sand; in the lower part, with an admixture of medium-grained sand; in the upper part, with interlayers of loamy sand; numerous in situ decomposed grass roots; horizontal, slightly tilted, was vertical bedding; with ocherous streaks and mottles. The bedding is disturbed by a large tongue (> 1.1 m in the vertical direction, ⩾5 cm in width) penetrating into the underlying layer and composed of sand and loamy sand enriched in ocherous iron compounds, with numerous black iron–organic concentrations on side walls (Fig. 3). Thin layers are wavy, smoothly curved upward along the streak and dissected by closed cracks; they are complicated by interpenetration, flexures, and downward displacement of fragments. The upper boundary is sharply uneven, complicated by small (1.5–2 cm) streaks from the top in the core sample from the borehole. In pit 1/17, at a depth of 2 m, a large (0.5-m-wide and 0.4-m-deep) subsidence composed of tilted layers of loamy sand and sand was exposed; it is associated with depressions in the polygonal relief (Fig. 1*B*). The lower part contains sparse wavy horizontal ice lenses ⩽0.1–0.2 cm thick, which cut through layering and deformations, W = 18–22 %. In the upper part, thin lenticular structure parallel to the surface is observed, W = 31 %
4, 5.05–4.25	Tobacco-gray loamy sand (Fig. 2) with silty coatings; nests and streaks of light silty sand; in the upper part, inclusions of decomposed plant detritus and ocherous mottles. The horizon is broken by sand streaks into rectangular and platy blocks up to 4 cm in size in the lower part and 1–1.5 cm in size in the upper part. These streaks shape a cellular structure. The upper boundary is eroded, sloping, and complicated by large (7–10 cm). The cryogenic texture is massive and tilted lenticular-broken. Loamy sand cemented by ice has the water content W = 24–27 %; sand with schlieren ice, 54 %
3, 6.65–5.05	Alternation of light silty fine sand, greenish peaty loamy sand, and bluish gray loam. Deposits in frozen and thawed states with numerous bluish spots along *in situ* grass roots and with ocherous streaks a at the contacts of layers of different compositions. Layering is thin, frequent, horizontal and tilted and shearing, complicated by vertical and oblique wavy streaks from the top with a height of more than 10 cm. A large streak was identified in the layer in the core samples from a depth of 5.5–6.2 m; numerous breaks and displacements of blocks 0.5 × 1.5 cm in size at the bottom and 2 × 4 cm at the top of the layer (Fig. 3). The sediments contain blue concentrations of vivianite 0.1 cm in size and inwashed detritus of shrubs and mosses *Drepanocladus* sp. with radiocarbon date of 45 205 ± 400 (5827 $IGRAN_{AMS}$) BP. Massive and lenticular cryogenic structure; ice lenses at the bottom of the layer are thin (<0.1 cm); in the upper part, 0.2–0.4 to 1.0–1.5 cm, W = 21–23 %. The top of the layer in the frozen state is masked by ice lenses and is distinguished from the overlying layer by changes in the color of the thawed sediment and by finer texture of the overlying sediment layer
2, 7.0–6.65	Loamy sand, fine sand, and loam; gray and dark gray, with inclined sedimentation layering broken by streaks and oblique fractures into flattened blocks of 1 × 2.5–3 × 4 cm in size. Numerous black mottles along filiform roots in situ; blue concentrations of vivianite and lenses of alluvial decomposed plant detritus. Massive cryogenic structure, W = 29 %. The upper boundary is distinct, eroded, with streaks of ocherous sand
1, 8.8–7.0	Gray fine sand with multidirectional parallel and tilted sedimentation bedding; acute-angled fragments of clay (1 cm), with thin (⩽1 mm) tilted bedding and with small ripples from inwashed brown plant detritus (Fig. 2). The remains of cotton grass, dwarf shrubs, and green mosses of *Drepanocladus* sp., *Calliergon* sp., and *Brachythecium* sp. with radiocarbon date of 49 110 ± 610 (5828 $IGRAN_{AMS}$) BP. Massive cryogenic structure, W = 21–28 %. The upper boundary is smooth, gently sloping

lection and plant guides [*Kats et al., 1977*]. Radiocarbon ages were obtained at the Collective Use Center "Laboratory of Radiocarbon Dating and Electron Microscopy" of the Institute of Geography of the Russian Academy of Sciences (Moscow) and at the Center for Applied Isotope Studies, University of Georgia (USA) [*Reimer et al., 2013*].

These analytical methods allowed us to reveal the traces of sedimentary, early diagenetic, pedogenetic, syn- and epicryogenic processes of freezing, thawing, and weathering in the Late Pleistocene sediments, because we used separate sets of lithogenetic facies [*Romanovsky, 1977*] and cryolithological features identified in the core samples.

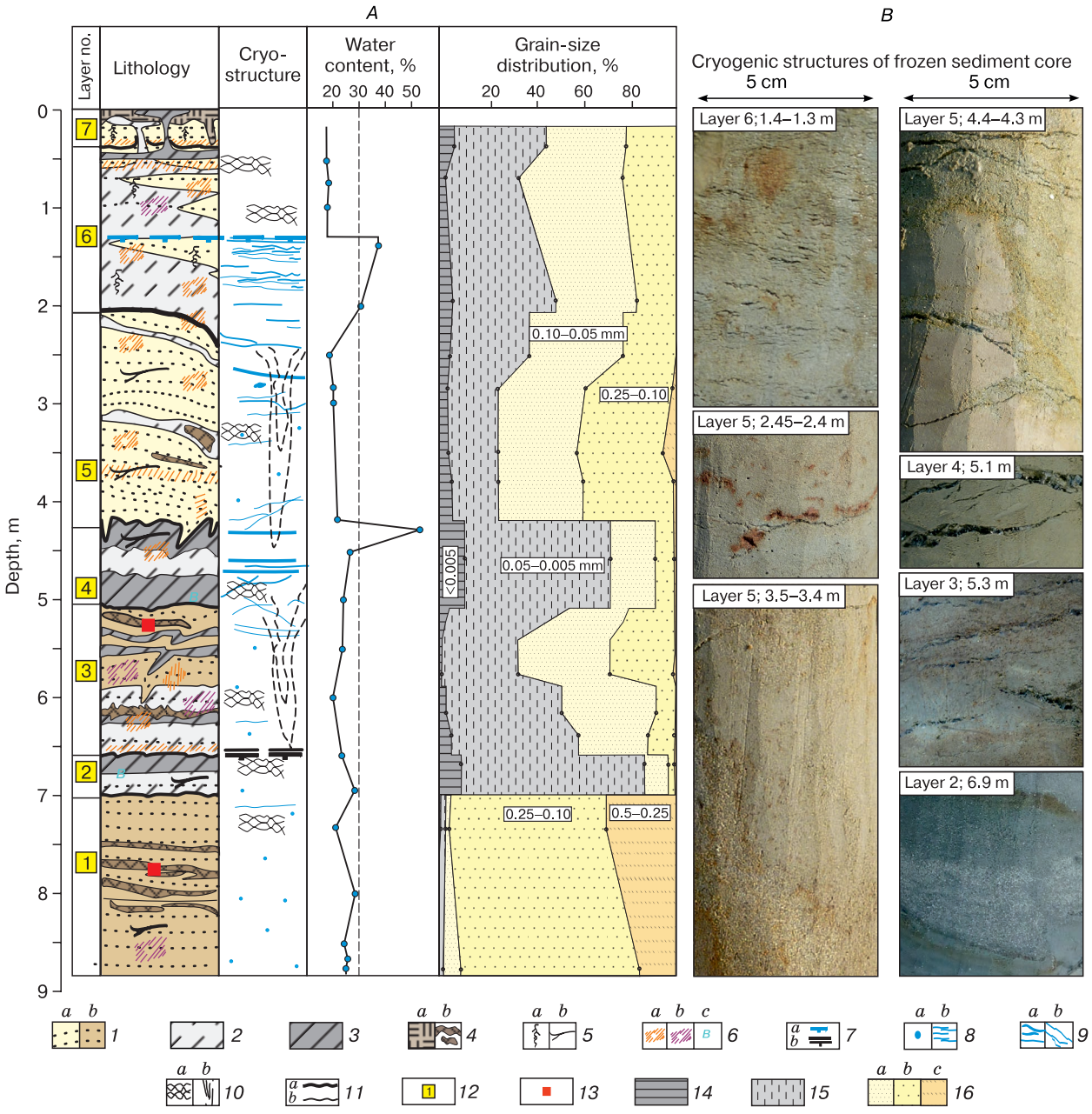

Fig. 2. Cryolithological structure of the third lacustrine–alluvial plain of the Pur-Taz interfluve according to sediment core data from borehole 1-16 (*A*) supplied with data from pits 1/17 and 1/18; cryogenic structures in the frozen sediment core (*B*, black color on photos corresponds to ice).

(*1*) yellowish (*a*) and gray (*b*) sand, (*2*) loamy sand, (*3*) loam, (*4*) autochthonous (*a*) and deposited by stream (alluvial) synchronously to growing (*b*) peat, (*5*) *in situ* plant roots and alluvial plant detritus (*b*); (*6*) ocherous-colored (*a*) and gray-colored (*b*) mottles and streaks and vivianite concentrations (*c*); (*7*) permafrost table (*a*) and base of relic talik (*b*); cryogenic structures: (*8*) massive (*a*) and micro- and thin lens-type (*b*); (*9*) layered, lens-type (*a*) and tilted broken lens-type (*b*); (*10*) post-cryogenic structures (*a*) and pseudomorphs (*b*); (*11*) boundaries of washout (*a*) and sediment layers (*b*); (*12*) layer number; (*13*) radiocarbon age sampling points. Grain-size fractions, mm: (*14*) clayey, (*15*) silt, (*16*) sand (*a* – very fine, *b* – fine, *c* – medium).

It is known that staged changes in frozen/thawed states of sediments appear as a variety of synchronous or superimposed cryogenic and post-cryogenic formations [*Romanovskii, 1993*] combined with the lithogenetic and facies features of the sedimentary stratum. To identify post-cryogenic formations, we analyzed signs of cryogenesis in the frozen and thawed parts of the section and data on grain-size dis-

tribution, mineralogical composition, and microstructure of sediments.

It is established [*Zigert, 1981; Konishchev and Rogov, 1985; Zigert and Slagoda, 1990; Slagoda, 2005; Rogov, 2009*] that multiple freeze–thaw cycles of syncryogenic sediments lead to (i) deformation of sedimentary layering and partial destruction of terrigenous particles and (ii) authigenic mineral formation and specific aggregation and ring-shaped microstructures that are preserved as post-cryogenic formations of different sizes after permafrost thawing. Layered, reticulate, and tilted broken lens-type cryogenic structures exist within epicryogenic permafrost. Initial post-cryogenic structures and early diagenetic structure elements may also persist [*Slagoda et al., 2015*]. Thawing of epicryogenic sediments can lead to (i) closure of ice voids, (ii) formation of post-cryogenic structure patterns as a result of discontinuities and displacements of layers, (iii) compaction of sediment blocks, and (iv) ferrugination and new formation of minerals [*Slagoda and Kurchatova, 2008; Slagoda et al., 2014*].

RESULTS

The structure of the upper part of permafrost corresponding to the third lacustrine–alluvial terrace in the northeast of the Pur-Taz interfluve and the results of analytical studies are shown in Figs. 2 and 3. We have used different data for determining the dynamics of sediment deposition environment [*Reineck and Singh, 1981*]: (i) grain-size distribution summarized on R. Passega's diagram (Fig. 4*A*), (ii) grain roundness, (iii) layering characteristics and the presence of washout within the section. We used chemistry of water extracts and the composition of plant remains to substantiate facies conditions of deposition.

Sediments of layers 1–3 were associated with the influence of a permanent stream of moderate to low intensity, possibly gradually becoming shallow. This was concluded given the (i) sedimentary layering, (ii) small wave ripples and deposition of detritus, (iii) elevated content of medium-grained particles at the bottom and small-grained particles in the upper part, (iv) decline of grain-size median values (M_d) from 0.215 to 0.04–0.02 mm and the sorting factor (So) increase from bottom to top within the section, and (v) the position of the samples on the diagram (Fig. 4*A*). Sediments were nonsaline: the sum of soluble salts was 88–258 mg/kg or 0.01–0.03 %. The concentrations of ions of soluble salts were in as follows: $Cl^- < HCO_3^- < SO_4^{2-}$ or $SO_4^{2-} < Cl^- < HCO_3^-$ for anions and $Mg^{2+} < Ca^{2+}$ for cations. These sediments layers were formed in subaerial conditions, most likely in the forest-tundra or northern taiga zones according to the composition of soluble salts and the set of plant remains, including mosses (Table 1) growing on wetlands, peatlands, and old trees. Layer 3 differed from the underlying layers by the presence of deformations, large streaks, predominance of acute-angled clastic particles with fresh cleavages (Fig. 4*B*), and ocherous coloration in the frozen state owing to the presence of iron hydroxides. Sediments of layers 1–3 deposited were 49–45 ka BP, in the first half of the Karginsky (middle Wisconsin) period.

Sediments of layer 4 were characterized by the uneven disturbed sedimentary layering, fine-grained composition (M_d = 0.031 mm), and high sorting factor values (So = 2.1). On the diagram, this sample lies in the area of homogeneous suspensions, which allowed us to identify it as the sediment of the reservoir (likely, lake sediment) with low flow regime.

Layers 5 and 6 are composed of silty sands (M_d = 0.064–0.099 mm) with the disturbed layering structure, with So values varying from 1.7–1.9 to 1.9–2.2, respectively. On the diagram (Fig. 4*A*) these sample lie within the areas of homogenous and gradational suspensions, which corresponds to the sediments of surface flows and permanent streams with low intensity on slopes.

Layer 7 belongs to active layer and is composed of sands and loamy sands (M_d = 0.074–0.08 mm; So = 1.9–2.3) disturbed by numerous cryoturbations and plant roots.

Taking into account these features, we have identified the following lithogenetic types in the section: layers 1 and 2 belong to stream channel alluvium; layer 3 with the disturbed sedimentary layering belongs to floodplain alluvium; layer 4 consists of sediments deposited in the water reservoir with low-flow stream; and layers 5, 6, and 7 are deluvial (slope washout, sheet erosion) or proluvial (erosion by temporary streams) (colluvial) sediments of temporary streams of low intensity (alluvial fans).

According to mineralogical composition, sediments of the entire section are dominated by feldspar and quartz grains. The sediments contain biotite, muscovite, epidote-zoisite, tourmaline, leucoxene, redeposited green glauconite, charcoal particles, fragments of diatoms, and sponge spicules. Terrigenous components could come from the erosion of Jurassic, Cretaceous, and Paleogene rocks and Quaternary marine sediments in this region.

Quartz grains in layers 1 and 2 are mainly angularly rounded, rarely cracked in situ. In layers 3–7, acute-angled and angular-rounded fragments, fractured, and with traces of dissolution and regeneration predominated. Fine-grained part of the sediments consists of the mixture of clay minerals: illite, chlorite, and mixed-layered aggregates with an admixture of siliceous and organic residues (Figs. 5*a*–5*g*; Fig. 6*a*). Clastic components and microaggregates are covered with thin discontinuous films of clay minerals (Figs. 6*b* and 6*d*). These features of the sediment composition are associated with post-sedimentary transformation.

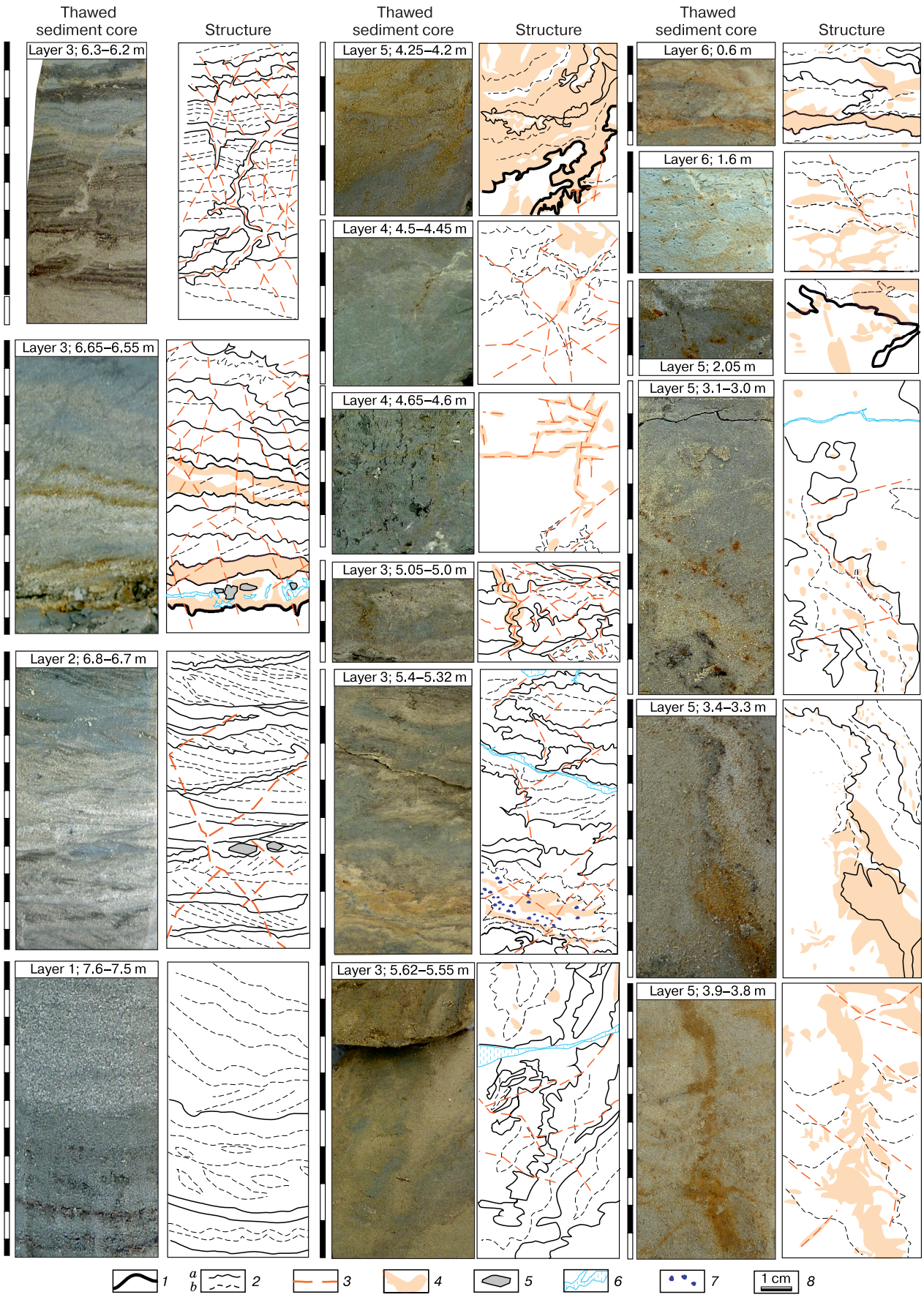
Thawed sediment core
Structure
Thawed sediment core
Structure
Thawed sediment core
Structure
Layer 3; 6.3–6.2 m
Layer 3; 6.65–6.55 m
Layer 2; 6.8–6.7 m
Layer 1; 7.6–7.5 m
Layer 5; 4.25–4.2 m
Layer 4; 4.5–4.45 m
Layer 4; 4.65–4.6 m
Layer 3; 5.05–5.0 m
Layer 3; 5.4–5.32 m
Layer 3; 5.62–5.55 m
Layer 6; 0.6 m
Layer 6; 1.6 m
Layer 5; 2.05 m
Layer 5; 3.1–3.0 m
Layer 5; 3.4–3.3 m
Layer 5; 3.9–3.8 m
1
a
b
2
3
4
5
6
7
1 cm
8

Fig. 3. Macrostructures and deformations in thawed sediment core from borehole 1-16:

(*1*) boundaries of washout between layers; (2) abrupt (*a*) and gradual (*b*) lithological boundaries; (*3*) zones of shifts, displacements of fragments, and layer breaks along closed and filled voids; (*4*) ocherous-mottles; (*5*) angular clay pellets; (*6*) voids from thawed ice lenses; (*7*) vivianite; (*8*) scale bar (unit – 1 cm).

DISCUSSION

We have revealed various cryogenic and post-cryogenic formations and defined their synchronous and superimposed character based on the obtained results of lithogenetic and facies features of sediments. The increase in the silt fraction content and the predominance of acute-angled clastic particles in floodplain, lacustrine, and colluvial cryogenic comminution under syngenetic freezing. Within the sediments, we have revealed in situ thawed and subsequently frozen sediments characterized by initial cryogenic and superimposed post-cryogenic structures and other features. Three groups of features can be distinguished:

1) Post-cryogenic macrostructures corresponding to the first stage of freeze–thaw cycle: blocky, reticulate, subangular blocky aggregates with iron oxide films, as well as complex multi-order aggregate and ring-shaped microstructures identified in the thin sections, fractures, and acute-angle clastic grains.

2) Gradual and abrupt (possibly along cracks) displacements of layer fragments relative to one another (mainly associated with thawing and early diagenetic transformation of thawed sediments), ruptures, streaks, and filling of voids with sediments from overlying horizons; deformations of sedimentary layering upon subsidence of sediments, and wavy, scalloped boundaries of layers (due to the compaction of multi-order aggregates).

3) Cryogenic structures corresponding to the last stage of freezing: inclusions of ice and voids from their thawing in the sediment core.

Stream channel sediments (layers 1 and 2) are characterized by bluish gray color of sands associated with reducing conditions and high water content. The frequency of small disturbances in layered macrostructure in the form of cracks, shears, and crushing of small ripples (Fig. 3) increases from the bottom to the top in the section of these two layers, especially within the interlayers of silty sands with plant remains. The microstructure of the sediments is characterized by (i) vertical fractures of thin interlayers without displacement, (ii) enrichment of the fracture zones with clastic particles from the overlying layers, and (iii) depletion in clay particles (probably, due to melting of ice inclusions). Sediment deposition was accompanied by in situ cracking of quartz grains during freeze–thaw cycles (Fig. 5*g*).

Authigenic minerals in these layers are mainly represented by carbonates: high-magnesian calcite and siderite. High-magnesian calcite forms dense microcrystalline spherical aggregates, often with an ad-

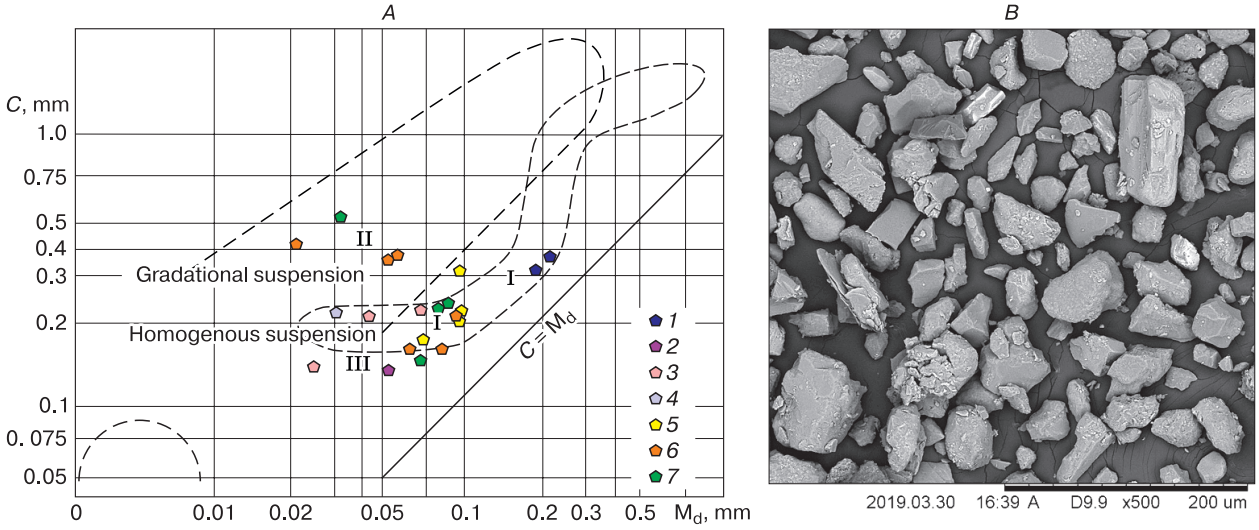

Fig. 4. Passega's diagram [*Reineck and Singh, 1981*], lithogenetic sediment types of the third lacustrine–alluvial plain of the Pur-Taz interfluve (*A*) and roundness of clastic particles in layer 3 (depth 6.4 m) (*B*).

M_d – median (50 % of the content), *C* – maximum diameter (99 % of the content); I – permanent stream alluvium, riverbed and floodplain alluvium (layers 1–3); II – subaerial delta sediments, colluvium (proluvium and deluvium) of temporary water streams (layers 5–7); III – sediments of exorheic water reservoirs (layer 4). Figurative sediment points of borehole 1-16 and pits: (*1*–*7*) – layers 1–7.

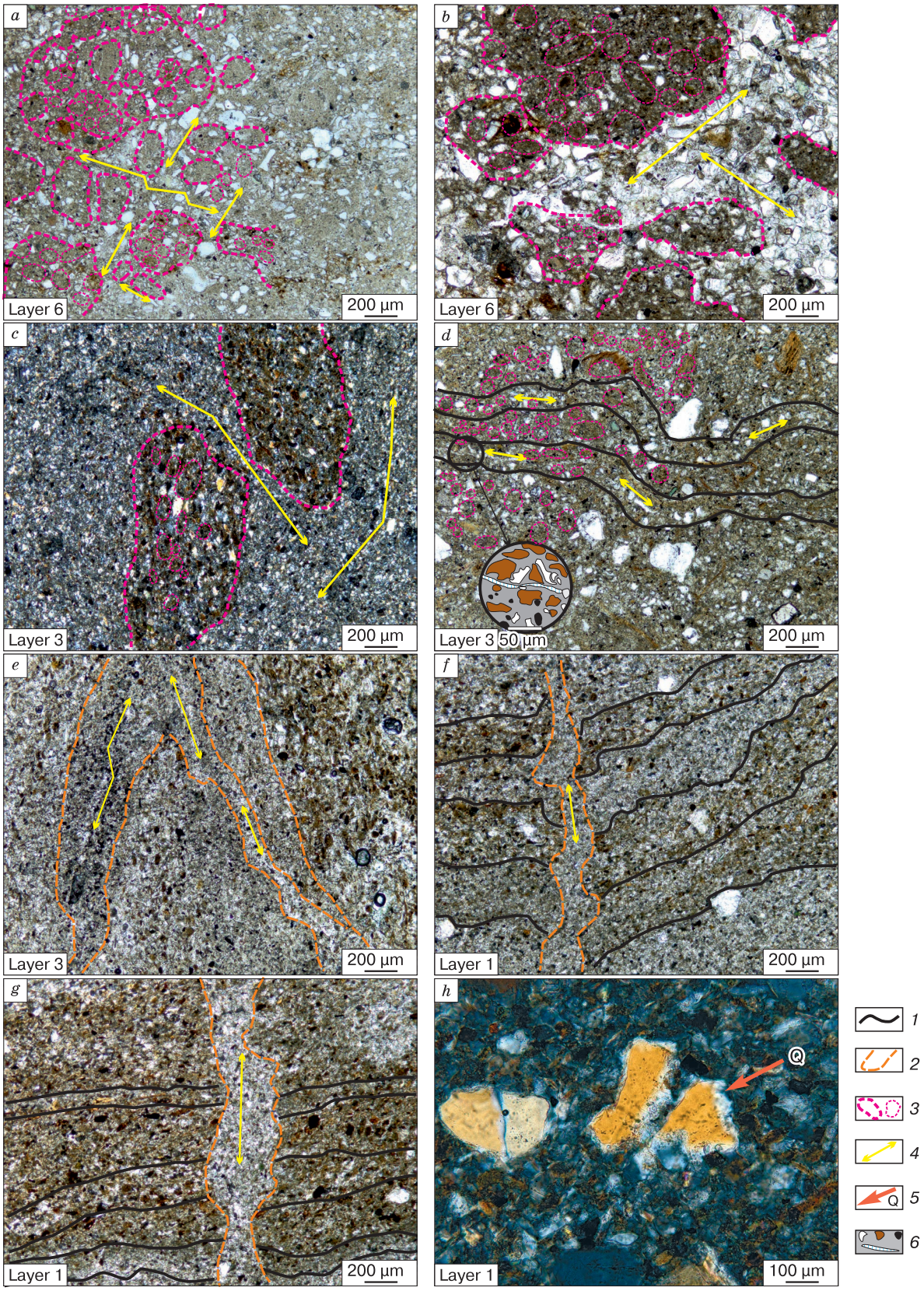
a
Layer 6
200 μm
b
Layer 6
200 μm
c
Layer 3
200 μm
d
Layer 3
50 μm
200 μm
e
Layer 3
200 μm
f
Layer 1
200 μm
g
Layer 1
200 μm
h
Q
Layer 1
100 μm
1
2
3
4
5
Q
6

Fig. 5. Microstructure of sediments from borehole 1-16 on photos of thin sections in transmitted light (*a, b, d–g*) and polarized light (*c, h*):

(*1*) boundaries of layers, (*2*) boundaries of microstructures and streaks, (*3*) boundaries of complex aggregates, (*4*) assumed directions of melt water flows and displacement of sediment components, (*5*) quartz (Q) fractured *in situ*, (*6*) relationships between fragments, aggregates, organic compounds, and voids on the inset picture (*d*).

mixture of aluminosilicate minerals, with relics of high-carbon biofilms (Figs. 6*c* and 6*g*). Such aggregates could be formed as a result of the mineralization of extracellular polysaccharide substance (EPS), one of the metabolic products of bacterial colonies and algae [*Trichet et al., 2001; Obst et al., 2009*]. Siderite is present as pelitomorphic microconcretions, mainly mixed with authigenic clay minerals developed over decomposing organic remains or highly hydrated micaceous material (Fig. 6*e*) [*Ruban et al., 2020; Raudina et al., 2021*].

In layer 2, disturbances in the macro- and microstructures of alluvial sediments form a discontinuous reticulate pattern along the thawed ice lenses. Therefore, they are classified as post-cryogenic microstructures. The preservation of fresh remains of mosses is usually associated with rapid freezing. The aforementioned authigenic minerals, elementary rounded clay aggregates, sulfate composition of soluble salts, and bluish coloration characteristic of reducing conditions within the talik are probably due to the secondary epigenetic freezing of the stream channel alluvium.

Floodplain alluvium (layer 3) includes a large streak with a vertical length of about 0.7 m. This layer has a reticulate-blocky macrostructure (Fig. 3) (a reticulate pattern of cracks dissecting and shifting sediment layers) and the corresponding multi-order complex aggregate and ring-shaped microstructures of mineral particles and clayey mass, as well as cross-orientation of thin films of mica. The streak contains vertically elongated lens-type aggregates (Figs. 5*c* and 5*e*). We have observed microvoids with crusts of clayey microaggregates on the walls within the thin interlayers and cavities infilled with clastic particles resulting from the thaw of ice lenses (Figs. 5*d* and 5*e*).

The authigenic minerals are mainly represented by vivianite and rhodochrosite within the interlayers enriched with plant residues. Vivianite with an admixture of manganese composes fine acicular microaggregates and cements adjacent fragments (Fig. 6*h*). Ferruginous rhodochrosite forms massive, sheaf-like aggregates and crusts of microcrystals covering the fragments (Fig. 6*e*). Given the shape and arrangement of rhodochrosite aggregates, this mineral was formed during crystallization of bacterial polysaccharide films, which acted as a substrate and catalyst for the deposition of mineral substances [*Leonova et al., 2017*].

Above described post-cryogenic macro- and microstructures are relics of cryogenic structure and ice wedge formation during syngenetic freezing of floodplain alluvium. They were formed after thawing of frozen ground with the development of ice wedge casts whose fragments are represented in the sediment core as a large streak. In situ thawing and subsidence of sediments was accompanied by the deformations of layering, macro- and microstructures. The authigenic minerals and ocherous coloration were associated with the transformation of thawed sediments and biological activity. Cryogenic structures and generally low water (ice) content in this layer were associated with its further epigenetic freezing.

Reservoir sediments (layer 4) overlay the floodplain alluvium. These are fine-grained sediments without distinct layering and with numerous remains of diatoms. Possibly, the talik existed during the sedimentation in reservoir and the floodplain sediments of layer 3 were partially thawed. Reticulate-blocky cryogenic structure was formed after the reservoir drainage. Sizes of preserved blocks of post-cryogenic structure increase from the top to the bottom of layer 4 indicating the epigenetic freezing of sediments. The macrostructures are emphasized by sandy streaks and iron oxide compounds between blocks of fine-grained sediments (Fig. 3). They are considered post-cryogenic structures formed during the thawing stage. Vivianite aggregates were formed in the thawed sediments during the decomposition of organic matter. Broken-lens type cryostructure of layer 4 is associated with subsequent epigenetic freezing.

Colluvial (deluvial and proluvial) sediments (layer 5) are marked by a large (>1.1 m in size) streak, the walls of which are cemented by iron compounds. At the contact with the streak in its lower part, the sedimentary layering is slightly convex (Fig. 2). Such patterns are typical for enclosing sediments with syngenetic ice wedges and pseudomorphs [*Shmelev, 1966*]. Numerous dense concentrations of iron oxides and iron–organic compounds reaching 0.5–1 cm in size (Figs. 2 and 3) are present in sands. We have also detected a lens type–reticulate macrostructure marked by streaks of iron oxides from thawed ice lenses. The scalloped wavy boundaries of layers were probably formed during the compaction of sediments with complex multi-order microstructures. The abovementioned layering disturbances, the structure of the streak, and its relationship with the enclosing sediments can be associated with the stage of accumulation, syngenetic freezing, and growth of ice wedges within colluvial sediments. During the thawing stage, pseudomorphs and post-cryogenic structure of enclosing sediments, as well as a set of authigenic iron

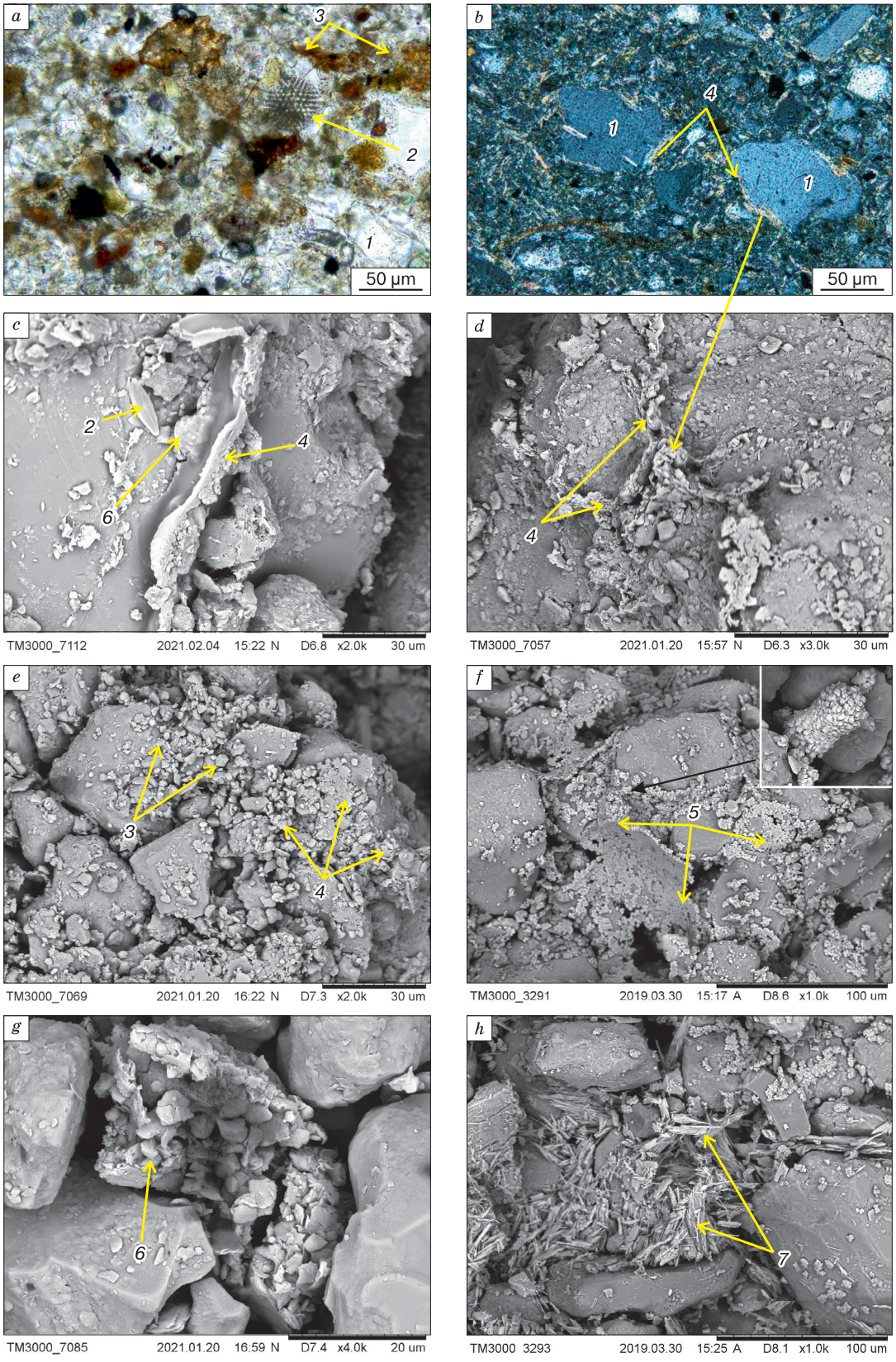
a
3
2
1
50 μm
b
4
1
1
50 μm
c
2
4
6
TM3000_7112 2021.02.04 15:22 N D6.8 x2.0k 30 um
d
4
TM3000_7057 2021.01.20 15:57 N D6.3 x3.0k 30 um
e
3
4
TM3000_7069 2021.01.20 16:22 N D7.3 x2.0k 30 um
f
5
TM3000_3291 2019.03.30 15:17 A D8.6 x1.0k 100 um
g
6
TM3000_7085 2021.01.20 16:59 N D7.4 x4.0k 20 um
h
7
TM3000 3293 2019.03.30 15:25 A D8.1 x1.0k 100 um

Fig. 6. Authigenic minerals in sediment core from borehole 1-16 on photos of thin sections in transmitted (*a*) and polarized (*b*) light; scanning electron microscopy (*c*–*h*):

concretions of pelitomorphic siderite over plant remains, fragments of diatom skeletons (*a*, layer 1); discontinuous films of authigenic clay minerals on quartz grains (*b*, layer 3; *d*, layer 1); microconcretions of dolomite and aluminosilicates over high-carbon organic films (*c*, layer 3); association of rhomboid microcrystals of siderite and clay minerals (*e*, layer 6); concentrations of split sheaf-like microcrystals of ferruginous rhodochrosite (*f*, layer 3); a fragment of a spherical aggregate of dolomite (*g*, layer 6); acicular columnar microcrystals of vivianite (*h*, layer 3). *1* – quartz, *2* – diatom shells, *3* – siderite, *4* – clay minerals, *5* – rhodochrosite, *6* – dolomite, and *7* – vivianite.

compounds characteristic of aerated conditions were formed. Cryogenic structures and low water content in this layer are associated with the subsequent epigenetic freezing of the drained sediments.

Colluvial (deluvial) sediments (layer 6) have a high content of silty particles and are colored in yellow and orange in frozen and thawed state. They have a blocky and cellular macrostructure marked by intersecting bands of iron oxides, scalloped boundaries, and displacements of layers along fractures resulting from melting ice lenses (Fig. 2, depth 1.3 m; Fig. 3, depth 1.6 m). These features correspond to a heterogeneous microstructure: (i) large disparate complex multi-order aggregates enriched in silt and clay and separated by fine streaks of sand and silt particles and (ii) numerous small complex aggregates surrounded by silty particles, as well as elementary clayey microaggregates (Figs. 5*a* and 5*b*). The authigenic minerals in the sediments are mainly represented by iron oxides, less often by pelitomorphic siderite formed after decomposed plant remains (Fig. 6*a*). Iron oxides mixed with aluminosilicates form thin discontinuous films on minerals and simple microaggregates (Figs. 6*b* and 6*d*).

These macro- and microstructures were apparently formed at the stage of syngenetic freezing of colluvial sediments. Though large streaks were not found in this layer in the sediment core, the traces of sediment subsidence caused by thawing were described at the bottom of layer 6 in the excavated pit. It is probable that this thaw think was formed above the thawed ice wedge, which corresponds to the polygonal surface topography. At the stage of thawing of layer 6, deformations of its layering, post-cryogenic macro- and microstructures, and authigenic minerals typical for aerated conditions were formed.

Active layer (layer 7) is characterized by numerous cryoturbations, ocherous coloration, and post-cryogenic lens–reticulate macrostructure i with displacements of layers along closed fractures (Fig. 3, depth 0.6 m). Interlayers with inflections, displacements, and scalloped boundaries were formed during the compaction of loamy sands with a multi-order aggregate microstructure while melting of ice lenses during freeze–thaw cycles.

It is known that stadial changes of frozen/thawed states of sediments are reflected as combinations of macro- and microstructures of different scales, deformations, and new formations [*Ershov, 1988*]. Our study has allowed determining the genesis of sediments and deposition conditions, as well as identifying the traces of post-sedimentation processes taking into account different groups of lithological features: (a) cryogenic macro- and microstructures transformed into post-cryogenic structures during thawing and melting of ice lenses; (b) deformations of sediment layering, including large streaks with vertical wavy layering that can be attributed to pseudomorphs; (c) fractured and acute-angled quartz grains that could appear during syncryogenic freezing. Complexes of ground wedges (pseudomorphs with vertical size up to 1.2 m) were observed on the third lacustrine–alluvial terrace in a quarry in 2021 (in floodplain sediments of Karginsky age) and in the exposure of the Taz River bank (in colluvial sediments). This confirms the interpretation of large streaks as pseudomorphs in the sediment core.

Some post-depositional changes (post-cryogenic structures, streaks, and deformations) resulted from the subsequent thawing and subsidence processes. The group of authigenic minerals in these sediments, as well as the decomposition of organic remains under the impact of microbiological activity can be attributed to superimposed early diagenetic processes in thawed sediments. The ocherous coloration of the sediments due to the neoformation of iron oxides and carbonates is associated with oxidation conditions in aerated thawed moist sediments. Except for the active layer, modern cryogenic structures were superimposed over thawed sediments during the last stage of epigenetic freezing of the Late Pleistocene sediments. Based on the presented data, it can be assumed that the polygonal topography of the surface corresponds to large pseudomorphs within the colluvial and solifluction sediments of layer 5 is a projected or inherited (i.e., relic) topography. The polygons are displaced and elongated along the slopes, as are the upper parts of the pseudomorphs, which slid down while the massif was displaced.

CONCLUSIONS

Specific features of the cryogenic and post-cryogenic macro- and microstructures in the studied sediments allows us to identify stadial changes in frozen/thawed states of the massif and to determine freezing types in stream channel, floodplain, and lacustrine

sediments of the early Karginsky age and in colluvial (deluvial and proluvial) sediments of the, presumably, Karginsky–Sartansky age. We propose the following model of these stadial changes in the north of the Pur–Taz interfluve.

1. Riverbed sediments of the Early Karginsky age could possibly undergo seasonal freezing-thawing under the low water conditions. This is evident from the cracking of quartz grains. These sediments were then subjected to epigenetic freezing in the upper part of the talik and have remained in the frozen state until now.

2. Floodplain syncryogenic sediments of the Early Karginsky age could possibly contain ice wedges. Their upper part could partially be washed away and the lower part was subjected to thawing and subsidence in the talik under the water reservoir with the formation of large vertical streaks (pseudomorphs) with their subsequent epigenetic freezing.

3. The sediments of the reservoir were initially thawed. Given the pattern of post-cryogenic structures, they were subjected to epigenetic freezing from the top, which could take place after drying of the reservoir. Later, they thawed out again together with the overlying sediment layers; then, their epigenetic freezing took place.

4. Colluvial (deluvial and proluvial) sediments had been accumulating in subaerial conditions of syngenetic freezing possibly during cold stages of the Karginsky–Sartansky age. They display post-cryogenic formations and large pseudomorphs–evidences of thaw and subsidence, which could take place at the end of the Sartansky period or in the Holocene. Then, these sediments were epigenetically frozen.

5. In general, the upper part of the geological section studied on the third lacustrine–alluvial terrace of the Pur-Taz interfluve consists of polygenetic sediments according to their deposition regime and types of freezing types. These sediments were subjected to thawing at least two times: (a) under the water reservoir (possibly, during the Karginsky period) and (b) during the Holocene climatic optimum. Their epigenetic freezing occurred during the climate cooling in the Late Holocene.

Acknowledgments. *This study was performed within the framework of state assignment No. 121041600042-7 using the equipment of the Collective Use Center "Bioinert Systems of the Cryosphere" at Tyumen Scientific Center, Siberian Branch of the Russian Academy of Sciences. A.A. Novoselov thanks the Ministry of Science and Higher education of the Russian Federation for supporting the project FEWZ-2020-0007.*

References

Ershov, E.D., 1988. Microstructures of permafrost. Moscow State University, Moscow, 182 p. (in Russian).

Ershov, E.D. (Ed.), 1989. Geocryology of the USSR. West Siberia. Nedra, Moscow, 454 p. (in Russian).

Google Earth, Landsat Data SIO.NOAA. U.S.Navy. NGA. GEBCO Image Landsat / Copernicus Image IBCAO https://earth.google.com/ (last visited: November 5, 2020).

Kats, N.Ya., Kats, S.V., Skobeeva, E.I., 1977. Atlas of Plant Remnants in Peat. Nedra, Moscow, 376 p. (in Russian).

Khomutov, A.V., Babkin, E.M., Tikhonravova, Ya.V. et al., 2019. Complex studies of the cryolithozone of the North-Eastern part of the Pur-Taz interfluve. In: Scientific Bulletin of the Yamalo-Nenets Autonomous District, vol. CII (2), p. 53–64 (in Russian).

Konishchev, V.N., Rogov, V.V., 1985. Methods of permafrost studies. Composition and cryogenic structures. Moscow State University, Moscow, 115 p. (in Russian).

Kurchatova, A.N., Rogov, V.V., 2014. Grain-size distribution and morphology of cryotic soils: new methods and approaches. Inzhenern. Izyskan., No. 5–6, 58–63 (in Russian).

Kurchatova, A.N., Rogov, V.V., 2020. Electron Microscopy in Geocryology. Moscow; Tyumen, MSU–TIU, 240 p. (in Russian).

Leonova, L.V., Kuzmina, L.Yu., Ryabova, A.S. et al., 2017. Experimental precipitation of Mg-containing bicarbonates in laboratory conditions. In: Mineralogy of technogenesis. Institute of Mineralogy UB RAS, Miass, No. 16, 200–207 (in Russian).

Obst, M., Dynes, J.J., Lawrence, J.R. et al., 2009. Precipitation of amorphous $CaCO_3$ (aragonite-like) by cyanobacteria: A STXM study of the influence of EPS on the nucleation process. Geochim. Cosmochim. Acta, No. 73, 4180–4198.

Raudina, T., Loiko, S., Kuzmina, D. et al., 2021. Colloidal organic carbon and trace elements in peat porewaters across a permafrost gradient in Western Siberia. Geoderma **390** (8), 11497.

Reimer, P.J., Brad, E., Bayliss, A. et al., 2013. IntCal13 and Marine13 radiocarbon age calibration curves 0–50 000 year cal BP. Radiocarbon LV (4), 1869–1887.

Reinek, H.-E., Singh, I.B., 1981. Depositional Sedimentary Environments. With Reference to Terrigenous Clastics. Nedra, Moscow, 439 p. (in Russian).

Rogov, V.V., 2009. The Foundations of Cryogenesis. Academic Publishing House "Geo", Novosibirsk, 203 p. (in Russian).

Romanovskii, N.N., 1993. Fundamentals of Cryogenesis in the Lithosphere. Moscow State University, Moscow, 336 p. (in Russian)

Romanovsky, S.I., 1977. Sedimentological Foundations of Lithology. Nedra, Leningrad, 408 p. (in Russian).

Ruban, A., Rudmin, M., Dudarev, O. et al., 2020. The Formation of Authigenic Carbonates at a Methane Seep Site in the Northern Part of the Laptev Sea. Minerals **10**, 948.

Shmelev, L.M., 1966. Traces of permafrost in the Quaternary deposits of the West Siberian Lowland and their paleoenvironmental significance. In: Quaternary of Siberia. Nauka, Moscow, p. 429–437 (in Russian).

Slagoda, E.A., 2005. Micromorphological Signatures of Cryogenesis in Late Cenozoic Sediments: Implications for the History of Permafrost. Thesis of Doctoral Dissertation (Geology & Mineralogy). Tyumen, 48 p. (in Russian).

Slagoda, E.A., Kurchatova, A.N., 2008. Micromorphological Analyses of Main Genetic Permafrost Types in West Siberia. In: Proceedings of Ninth International Conference on Permafrost (Fairbanks, June 28 – July 3, 2008). Fairbanks, University of Alaska (Fairbanks), vol. II, p. 1659–1663.

Slagoda, E.A., Kurchatova, A.N., Popov, K.A. et al., 2014. Cryolithologic structure of the first terrace: Microstructure and evidence of cryolithogenesis, Bely Island, Kara Sea (Part 2). Earth's Cryosphere XVIII (1), 12–22.

Slagoda, E.A., Krylov, A.V., Popov, K.A. et al., 2015. Permafrost in Hayes Island, Franz Josef Land Archipelago. Earth's Cryosphere XIX (4), 17–28.

Slagoda, E.A., Tikhonravova, Ya.V., Kuznetsova, A.O., Koroleva, E.S., 2019. Cryoturbations, pseudomorphs, postcryogenic textures and involutions in the frozen sediments of the Pur-Taz interfluve. In: Proceedings of the International Conference "Solving the puzzles from Cryosphere" (Pushchino, April 15–18, 2019). Pushchino, "Okabiolab" Ltd., p. 109–110.

Tikhonravova, Ya.V., Slagoda, E.A., Rogov, V.V. et al., 2020. Heterogeneous ices in ice wedges structure on the Pur-Taz interfluve peatlands of the North of West Siberia. Led i Sneg LX (2), 225–238 (in Russian).

Trichet, J., Defarge, C., Tribble, J. et al., 2001. Christmas Island lagoonal lakes, models for the deposition of carbonate-evaporite organic laminated sediments. Sediment. Geol., No. 140, 177–189.

Trofimov, V.T., Badu, Yu.B., Vasil'chuk, Yu.K., Kashperyuk, P.I. et al., 1987. Geocryological zoning of the West Siberian plate. Nauka, Moscow, 221 p. (in Russian).

Vasil'chuk, Yu.K., Vasil'chuk, A.C., 2016. Thick polygonal peatlands in continuous permafrost zone of West Siberia. Earth's Cryosphere XX (4), 3–13 (in Russian).

Zigert, Kh.G., 1981. Mineral formation in periglacial conditions. In: Structure and Thermal Regime of Permafrost. Nauka, Novosibirsk, p. 14–21 (in Russian).

Zigert, Kh.G., Slagoda, E.A., 1990. Results of Ice Complex' studies in Yakutia. In: Quaternary Stratigraphy and Events in Eurasia and Pacific Regions. YaSC, Yakutsk, p. 82–84 (in Russian).

Zykina, V.S., Zykin, V.S., Volvakh, A.O. et al., 2017. Upper Quaternary deposits of the Nadym-Ob area: stratigraphy, cryogenic formations, and deposition environments. Earth's Cryosphere XXI (6), 12–20.

Received April 22, 2021
Revised November 24, 2021
Accepted January 16, 2022

Translated by Yu.A. Dvornikov